J. Fluid Mech. (1996), vol. 324, pp. 261 286

Non-isothermal spreading of a thin liquid film on an inclined plane

By P. GILBERTO LÓPEZ, S. GEORGE BANKOFF AND MICHAEL J. MIKSIS

McCormick School of Engineering and Applied Science, Northwestern University, Evanston, IL 60208, USA

(Received 28 March 1995 and in revised form 16 April 1996)

A thin layer of liquid advancing over a dry, heated, inclined plate is studied. A lubrication model with contact line motion is derived. The plate is at constant temperature, and the surface Biot number is specified. The steady-state solution is obtained numerically. In addition, the steady-state solution is studied analytically in the neighbourhood of the contact line. A linear stability analysis about the steady state is then performed. The effects of gravity, thermocapillarity and contact line motion are discussed. In particular, we determine a band of unstable wavenumbers, and the maximum growth rate as a function of these parameters.

1. Introduction

Many industrial processes involve the coating of a solid surface with a thin liquid film. In general, the solid surface or the film may be heated. These films can be driven by gravity, centrifugal force or an applied pressure. One problem that may arise during the initial wetting of the solid is for a spanwise instability to develop along the leading edge of the film (Williams 1977; Huppert 1982). This instability can exhibit itself in the form of fingers, or a sawtooth-like pattern. The appearance of the sawtooth pattern may not be harmful, since the solid can eventually become completely wetted. On the other hand, the fluid from the film can flow wholly within the fingers, leaving stable dry regions. Our aim here is to consider the coating of an inclined plane by gravity under non-isothermal situations. This case should have the features of many industrial coating processes, while allowing for comparison to experiments. Our primary concern will be to study the linear stability of the leading edge in a non-isothermal situation.

The instability of the leading edge of a sheet of viscous isothermal fluid flowing down an inclined plane has been illustrated in the experimental work of Huppert (1982). He observed cases where the leading edge developed either long parallel-sided fingers or where a sawtooth shape developed which moved down the inclined plane. Additional experimental work on this problem was done by Silvi & Dussan V. (1985). They observed a similar behaviour of the leading edge but also noted that the magnitude of the contact angle at the leading edge could explain the two leading-edge configurations. Hocking (1990) noted that, near the leading edge of the fluid, there is a hump whose height is considerably larger than that of the sheet some distance up the plane. This suggested that one could study the motion of a ridge of

fluid with both a leading and a trailing edge and capture the physics of the sheet problem. This analysis contained the effect of the contact line, in the quasi-steady limit. Hocking & Miksis (1993) again studied the ridge model, but followed the quasi-steady model into the nonlinear regime numerically, and determined conditions for the formation of droplets as a function of the contact angle and the other physical parameters. They also studied the ridge model without the quasi-steady assumption. In this case a linear stability analysis gave a preferred wavelength for the instability.

The linear stability problem for the leading edge of a fluid sheet was first studied by Troian *et al.* (1989). Their model did not have a contact line present, but there was a very thin film of fluid extending down the plane in front of the sheet. The leading edge was identified as the front of a narrow region where the height of the fluid changed from a slowly varying relatively thick layer to a very thin region. They showed that there was a preferred wavelength for linear stability of spanwise disturbances to the leading edge, and that this wavelength was only weakly dependent on the thickness of the film ahead of the edge. De Bruyn (1992) has confirmed experimentally some qualitative features of the theoretical predictions of Troian *et al.* As noted above, Hocking & Miksis (1993) also found a preferred wavelength in their ridge model. The introduction of the contact line motion in the model of Hocking & Miksis required that slip along the solid surface be introduced, in order to remove the force singularity at the contact line. The preferred wavelength depended weakly on the value of the slip coefficient, similar to the weak dependence of the Troian *et al.* model on the downstream thickness of the film.

Goodwin & Homsy (1991) have determined the steady-state profile of a film moving down an inclined plane at a constant velocity with no spanwise variation in the isothermal case. They solved the Stokes equations numerically with no-slip along the inclined plane. Hence they were not restricted by the small slope assumption of lubrication theory, but their solution did have the non-integrable stress singularity at the contact line. It is not clear how this approach can be extended to a dynamic situation. Also Schwartz (1989) has studied isothermal viscous flows down an inclined plane in the lubrication limit, assuming that the film completely wets the plane. He determined numerically the evolution of a disturbance along the film.

There has been a considerable amount of work on the dynamics of heated films. For example, thermocapillarity has been incorporated into falling films by Lin (1975), Sreenivasan & Lin (1978), and Kelly, Davis & Goussis (1986). Burelbach, Bankoff & Davis (1988) have considered the rupture of evaporating heated films. For a thin film on a heated inclined plane the interaction of the two modes of instability, namely hydrodynamic (or surface wave) and thermocapillarity instability, has been examined by Joo, Davis & Bankoff (1991), who developed an evolution equation for two-dimensional disturbances along a film interface. Their evolution equation accounts for the viscosity of the film, gravity, surface tension of the interface, thermocapillarity and evaporation effects.

The non-isothermal spreading of a liquid drop on a heated (or cooled) horizontal surface, accounting for the motion of the contact line, was first studied by Ehrhard & Davis (1991). They developed a lubrication model for the drop interface which included thermocapillary effects and contact line motion. One of their interesting results was that, for zero advancing contact angle, heating will prevent the drop from spreading to infinity. Ehrhard (1993) did a series of experiments on the spreading of non-isothermal drops and observed good quantitative agreement with the predictions of Ehrhard & Davis (1991).

We will develop a model in the non-isothermal lubrication limit for the motion of a fluid film down an inclined plane which accounts for the motion of the contact line. The presence of a contact line introduces a non-integrable stress singularity when the no-slip boundary condition is used at the plate (Dussan V. & Davis 1974). To eliminate this non-integrable stress singularity a Navier slip condition with a singular slip function (Greenspan 1978) is introduced along the solid surface. Changes in surface tension are introduced into the model, induced by temperature changes. The dependence of surface tension on temperature is introduced such that far from the contact line we recover the usual linear first approximation, but in the neighbourhood of the contact line the linear dependence is modified so that $d\sigma/dT = 0$ at the contact line. With these modelling assumptions the relevant physical quantities are all well-behaved functions at the contact line. We study the steady-state solutions that move down the plane at a constant velocity and with no spanwise variation. The linear stability of these states will then be determined as a function of the physical parameters. In addition, we will solve for the local behaviour of the interface in the neighbourhood of the contact line analytically and show how these analytical solutions can help predict the behaviour of the interface.

2. Formulation of the problem

Consider an infinite layer of liquid as it advances on a non-isothermal plane solid surface that makes an angle α with the horizontal. The liquid is modelled as a three-dimensional Newtonian non-volatile incompressible fluid surrounded by a passive gas. We choose our coordinate system (x, y, z) so that x and y lie in the plane, with x the down-slope coordinate. The free surface will be located at $z = h(x, y, t)$ where z is perpendicular to the plane (see figure 1).

The velocity and thermal fields are governed by the Navier–Stokes, continuity and energy equations:

$$\rho \left\{ \frac{\partial \boldsymbol{u}}{\partial t} + \boldsymbol{u} \cdot \nabla \boldsymbol{u} \right\} = -\nabla p + \mu \nabla^2 \boldsymbol{u} + \rho \boldsymbol{g}, \tag{2.1}$$

$$\nabla \cdot \boldsymbol{u} = 0, \tag{2.2}$$

$$\rho\, C_p \left\{ \frac{\partial T}{\partial t} + \boldsymbol{u} \cdot \nabla T \right\} = \beta\, \nabla^2 T. \tag{2.3}$$

In the above equations $\boldsymbol{g} = (g \sin\alpha, 0, -g\cos\alpha)$ denotes the acceleration due to gravity, α is the angle the inclined plane makes with the horizontal, $\boldsymbol{u} = (u, v, w)$ the velocity vector, p the pressure and T the temperature of the liquid. The density ρ, the viscosity μ, the heat capacity C_p and the thermal conductivity β of the liquid will be taken as constants.

Along the liquid–solid interface $z = 0$ the boundary conditions are those of an impenetrable, perfectly conducting surface:

$$w = 0, \tag{2.4}$$

$$T = T_0. \tag{2.5}$$

In order to eliminate the stress singularity at the contact line, we need to relax the no-slip condition (see e.g. Dussan V. 1979). This can be done by using a Navier-type

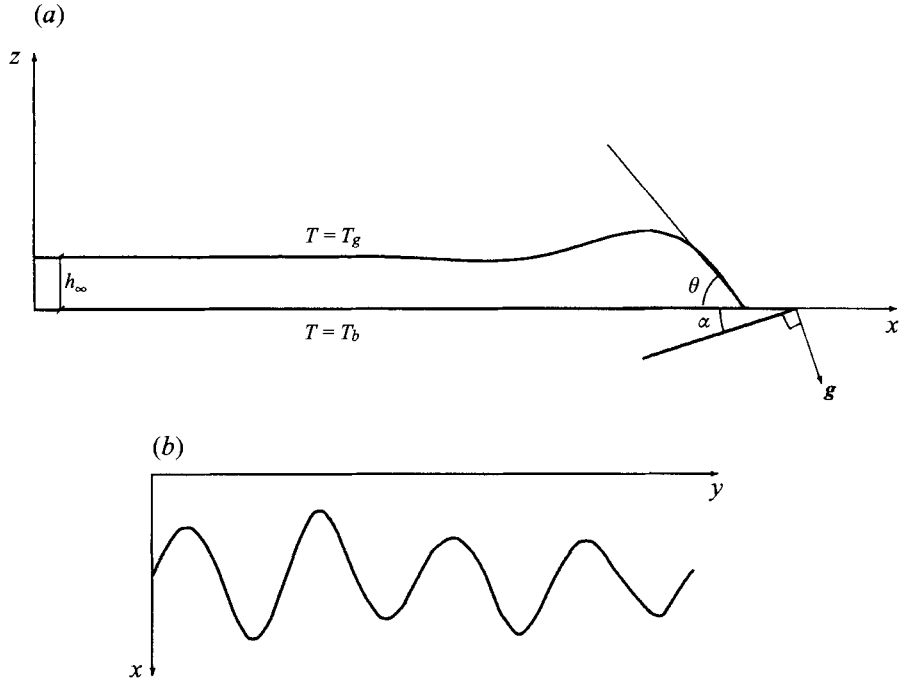

FIGURE 1. Geometry and coordinate system for a film flow down an inclined plane, (*a*) cross-section in the (*x*, *z*)-plane, (*b*) plan view of the (*x*, *y*)-plane.

slip condition along the solid interface:

$$u - \bar{\lambda}(h)\left(\frac{\partial u}{\partial z} + \frac{\partial w}{\partial x}\right) = 0, \quad v - \bar{\lambda}(h)\left(\frac{\partial v}{\partial z} + \frac{\partial w}{\partial y}\right) = 0. \tag{2.6a, b}$$

Here we will use a slip coefficient function $\bar{\lambda}(h)$ in equation (2) of the form

$$\bar{\lambda}(h) = \frac{\hat{\lambda}}{h}, \tag{2.7}$$

with $\hat{\lambda}$, the slip coefficient, a positive constant. This form of the slip coefficient function was introduced by Greenspan (1978) in his investigation of drop spreading. Different forms of the slip coefficient have been used but only small qualitative differences in the dynamics of the contact line are observed (Dussan V. 1976; Haley & Miksis 1991).

At the liquid–gas interface $z = h(x, y, t)$, we have the kinematic boundary condition:

$$w - \frac{\partial h}{\partial t} = u\frac{\partial h}{\partial x} + v\frac{\partial h}{\partial y} \tag{2.8}$$

and the conditions that the stress tensor $\boldsymbol{T}$ balances in the normal and tangential directions:

$$\boldsymbol{n} \cdot \boldsymbol{T} \cdot \boldsymbol{n} = 2\kappa\sigma, \tag{2.9}$$

$$\boldsymbol{\tau} \cdot \boldsymbol{T} \cdot \boldsymbol{n} = \boldsymbol{\tau} \cdot \nabla\sigma, \tag{2.10}$$

where $\boldsymbol{n}$ and $\boldsymbol{t}$ are the normal and tangential unit vectors, with $\boldsymbol{n}$ pointing out of the surface, while κ is the mean curvature of the surface. Condition (2.10) must be

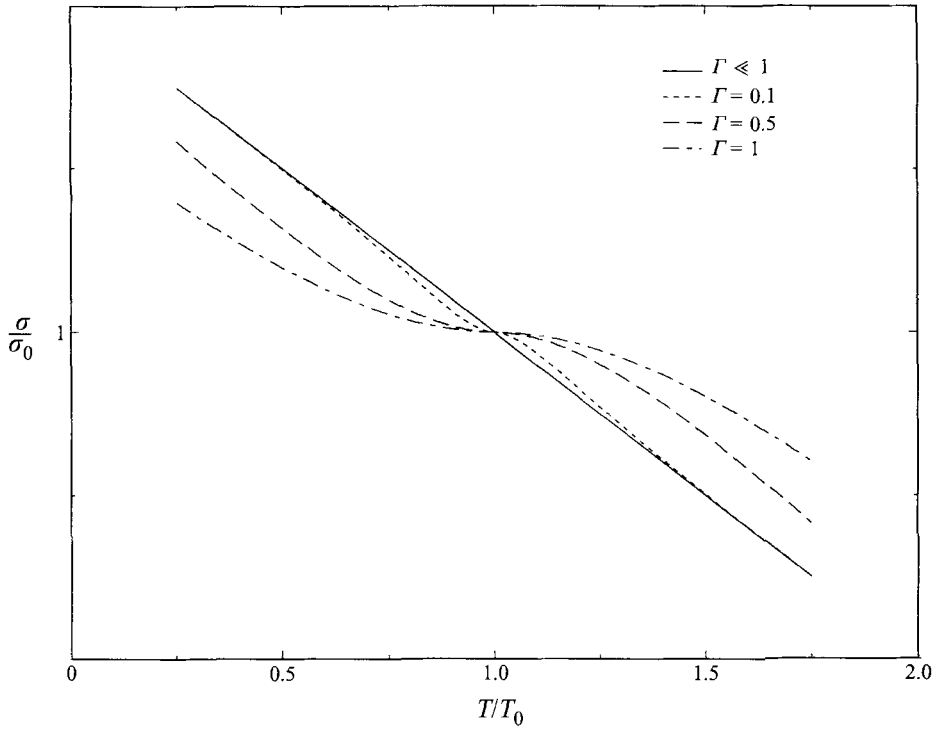

FIGURE 2. Dependence of the scaled surface tension σ/σ_0 on the scaled temperature T/T_0 for different values of the parameter Γ.

complemented by an equation of state for the surface tension:

$$\sigma = \sigma_0 - \gamma(T^I - T_0)\left(1 - \exp\left[\frac{-|T^I - T_0|}{\Gamma}\right]\right), \tag{2.11}$$

where σ_0 denotes the value of surface tension at the plate temperature T_0, T^I the temperature of the interface, γ is a positive constant and Γ is a small positive constant. Since we are heating the liquid from below, $T^I < T_0$ away from the contact line. Note that for Γ small, σ is approximately a linear function of the surface temperature T^I everywhere, except in a small neighbourhood of the contact line (figure 2). This linear dependence of surface tension on temperature is the usual first approximation. We have modified this approximation only in the neighbourhood of the contact line, where the exponential term in (2.11) forces $\mathrm{d}\sigma/\mathrm{d}T^I = 0$ there. This dependence of surface tension on temperature, along with the slip condition (2.6) and (2.7), make the fluid interface a regular function at the contact line. Hence we are not concerned about any singularities there. This regularity could have also been accomplished in the model by allowing the exponential term in (2.11) to depend on the film thickness or the distance from the contact line. The use of a modified equation of state for the surface tension is thus a mathematical device to obtain a regular problem at the contact line in the non-isothermal, non-evaporating case. However, physical arguments can be put in its favour. First, experimental measurements for a slowly advancing contact line (Truong & Wagner 1987; Cazabat 1991) and theoretical studies (Renk, Wayner & Homsy 1978; de Gennes 1985) have indicated the existence of a very thin 'foot' which serves as a bridge between the bulk liquid and the adsorbed layer on the 'dry'

solid. This implies a region of large curvature where the film thickness passes from a region of strong dispersion forces to one where such forces become weak compared to surface tension and gravitational forces. In this foot the fluid temperature is the same as the wall temperature, taken to be a constant. Hence the gradient of surface tension in this foot is $\nabla\sigma = (\mathrm{d}\sigma/\mathrm{d}T)\nabla T$. Outside this region, the surface tension varies linearly with temperature. Equation (2.11) conveniently describes this behaviour. One can also note that surface tension is no longer independent of film thickness for such ultrathin layers, and, in fact, is poorly defined.

The dynamics of the isothermal fluid in the neighbourhood of a contact line are very complicated, and the usual no-slip boundary condition results in a non-integrable stress singularity. One way to resolve this problem is to introduce slip at the plate in the form (2.6). In the case where $\bar{\lambda}(h)$ is a constant, integrable singularities are still present in the isothermal case. However, this is not the case when a slip function like (2.7) is used, so that the solution is regular. Hence linear stability of a fluid interface with a contact line can be discussed. When we consider thermocapillarity effects, condition (2.11) results in a regular problem at the contact line and allows a discussion of linear stability.

Following Ehrhard & Davis (1991) for a non-evaporating liquid ($T_g < T_s$, where T_s is the saturation temperature at the ambient pressure, p_g) the heat transfer at the liquid–gas interface is governed by a mixed-type condition,

$$\beta\frac{\partial T}{\partial n} + \frac{\beta_g}{\Delta}(T - T_g) = 0. \tag{2.12}$$

In this equation, n is the magnitude of the normal unit vector, β_g is the thermal conductivity of the gas at the constant temperature T_g, and Δ is the thickness of the thermal boundary layer within the gas. A heat transfer condition such as (2.12) at the interface permits us to study the limiting cases between an adiabatic and a perfectly conducting boundary.

The leading edge, or contact line, is located at $x = a(y,t)$. Here the boundary conditions are contact with the plate,

$$h = 0, \tag{2.13}$$

plus the definition of the apparent contact angle θ as the apparent angle the film interface makes with the solid surface $z = 0$, in the plane perpendicular to $z = 0$ and containing the normal vector to the contact line,

$$\tan\theta = -\frac{\partial h}{\partial x}\left[1 + \left(\frac{\partial a}{\partial y}\right)^2\right]^{1/2}. \tag{2.14}$$

We will assume a relationship between the slip velocity at the contact line, U_s, and the contact angle θ of the form

$$U_s = k(\theta - \hat{\theta}_s)^m \quad (m \geqslant 1), \tag{2.15}$$

where $\hat{\theta}_s$ is the static (advancing) contact angle and k an empirical positive constant. The origins of relationship (2.15) come from the experimental curves of contact angle *vs.* slip velocity (see for example Schwartz & Tejeda 1972). In these curves it is the apparent (measured) contact angle that is reported, as opposed to the actual contact angle θ. Nevertheless, we use (2.15) as our θ *vs.* U_s condition. Some additional discussion on this matter can be found in Dussan V. (1976) and Hocking (1992). The cubic dependence $m = 3$ is suggested by the experimental

results of Schwartz & Tejeda (1972) and Ehrhard (1993) and will be used later in the presentation of the results. When considering the spreading of a droplet with a contact line, Haley & Miksis (1991) and Ehrhard & Davis (1991), for the non-isothermal case, used different values of m (= 1, 3), without a relevant change in their results. The limiting case of a fixed contact angle, used by Hocking & Miksis (1993), for the ridge of fluid over an inclined plane, is contained in the present analysis when we let $k \to \infty$.

Finally a boundary condition is necessary at $x = -\infty$. Here we assume a film of uniform thickness h_∞. Hence as

$$x \to -\infty, \text{ then } h \to h_\infty \tag{2.16}$$

and all derivatives of h vanish.

We begin our study of the above equations by introducing dimensionless variables. Because the film has a uniform thickness at infinity, the volumetric flux per unit length Q_∞ (in the spanwise direction) is constant there and equals

$$Q_\infty = \frac{\rho g h_\infty^3}{3\mu}\left(1 + 3\frac{\hat{\lambda}}{h_\infty^2}\right)\sin\alpha. \tag{2.17}$$

This drives the motion of the interface down the inclined plane and introduces a velocity scale $U = Q_\infty/h_\infty$. The length scale in the direction perpendicular to the plane is h_∞. When we balance the hydrostatic pressure, a capillary length scale for the x- and y-coordinates can be chosen, $l = (\sigma_0/3\mu U)^{1/3}h_\infty$, and is expected to be much larger than the film thickness. The complete set of dimensionless variables is

$$\left.\begin{aligned}(\hat{x},\hat{y},\hat{z}) = \left(\frac{x}{l},\frac{y}{l},\frac{z}{h_\infty}\right), \quad \hat{h} = \frac{h}{h_\infty}, \quad (\hat{u},\hat{v},\hat{w}) = \left(\frac{u}{U},\frac{v}{U},\frac{wl}{Uh_\infty}\right),\\ \hat{t} = \frac{tU}{l}, \quad \hat{p} = \frac{l^2}{\sigma_0 h_\infty}(p - p_g), \quad \hat{T} = \frac{T - T_0}{T_0 - T_g} \quad \hat{\theta} = \frac{l}{h_\infty}\theta.\end{aligned}\right\} \tag{2.18}$$

The ratio of length scales is related to the capillary number

$$Ca = \frac{3\mu U}{\sigma_0} \tag{2.19}$$

by $h_\infty/l = Ca^{1/3}$. Our aim is to derive an evolution equation for the motion of the film interface in the lubrication limit, i.e.

$$\epsilon = h_\infty/l \ll 1. \tag{2.20}$$

Our analysis will parallel the work of Ehrhard & Davis (1991) who considered the spreading of a droplet. We first introduce the scaled variables (2.18) into the equations of motion (2.1)–(2.16). For example the heat transfer equation (2.3) becomes

$$Re\, Pr\, \epsilon\left\{\frac{\partial\hat{T}}{\partial\hat{t}} + \hat{\boldsymbol{u}}\cdot\hat{\nabla}\hat{T}\right\} = \epsilon^2\left(\frac{\partial^2\hat{T}}{\partial\hat{x}^2} + \frac{\partial^2\hat{T}}{\partial\hat{y}^2}\right) + \frac{\partial^2\hat{T}}{\partial\hat{z}^2}, \tag{2.21}$$

where the Reynolds number $Re = Q_\infty/\nu$ and the Prandtl number $Pr = \beta/\rho C_p \nu$ are assumed to be order-one quantities. Then we look for a solution in the form of a perturbation series in ϵ. We consider only the problem for leading order in ϵ, i.e. lubrication theory. For example, at leading order (2.21) implies that $\hat{T}$ is a linear function of z. These leading-order equations can then be integrated. The result is that all the leading-order dependent variables can be shown to be explicit functions of the

leading-order $\hat{h}$ and the independent variables. In addition, an evolution equation for the leading-order $\hat{h}$ can be determined. The resulting nonlinear evolution equation for the free surface is

$$\frac{\partial h}{\partial t} + \frac{\partial}{\partial x}\left\{\left(h^3 + 3\lambda h\right)\left((\nabla^2 h)_x - Gh_x + \frac{1}{1+3\lambda}\right) + M\Psi(h)\left(h^2 + 2\lambda\right)h_x\right\}$$

$$+ \frac{\partial}{\partial y}\left\{\left(h^3 + 3\lambda h\right)\left((\nabla^2 h)_y - Gh_y\right) + M\Psi(h)\left(h^2 + 2\lambda\right)h_y\right\} = 0, \quad (2.22)$$

where the hats have been dropped, h represents the term that is leading order in ϵ and ∇^2 is the two-dimensional Laplacian operator, $\partial^2/\partial x^2 + \partial^2/\partial y^2$. The term that contains the surface tension gradients due to the heating is represented by the function

$$\Psi(h) = \frac{1}{(1+Bih)^2}\left(1 - \left[1 - \frac{Ah}{1+Bih}\right]\exp\left\{\frac{-Ah}{1+Bih}\right\}\right). \quad (2.23)$$

A series of dimensionless parameters appear in equations (2.22) and (2.23) that contain the physical information of the model. The importance of the vertical pressure gradients with respect to the other forces is represented by the parameter G, defined by

$$G = \frac{Ca^{1/3}}{1+3\lambda}\cot\alpha, \quad (2.24)$$

while the scaled slip coefficient, λ, is given by

$$\lambda = \frac{\hat{\lambda}}{h_\infty^2}. \quad (2.25)$$

Note that for large inclination angles, $\alpha \approx \pi/2$, G can be neglected.

The Marangoni number M compares a characteristic change in surface tension, due to heating, to the surface tension at the plate temperature:

$$M = \frac{3\gamma(T_0 - T_g)l^2\beta_g}{2\sigma_0 h_\infty \beta\Delta}. \quad (2.26)$$

With this definition, M also contains the term that controls the heat flux at the liquid–gas interface, i.e. the Biot number Bi:

$$Bi = \frac{\beta_g h_\infty}{\beta\Delta}. \quad (2.27)$$

Using these definitions we can retain the thermocapillary effects even when the heat transfer is very poor at the free surface. The limit $Bi \to 0$ would be the case of no heat flux in the surface. Hence the dimensional temperature field is constant, with the value T_0. The other limiting case, $Bi \to \infty$, is appropriate for a perfectly conducting gas, so that the surface is maintained at a constant temperature, with dimensional value T_g. The parameter A, defined by

$$A = \frac{(T_0 - T_g)\beta_g h_\infty}{\Gamma\ \beta\Delta}, \quad (2.28)$$

is expected to be large (but the whole term must be retained in order to have thermocapillary effects), and contains the heat transfer coefficient. This parameter A defines a small region of rapid change between a linear variation in surface tension

with temperature, where $d\sigma/dT = -\gamma$, and $d\sigma/dT = 0$ at the contact line. For a heated plate $T_0 - T_g > 0$ and hence all of the dimensionless parameters are positive.

To leading order in ϵ, the boundary conditions at the contact line $x = a(y,t)$ are

$$h = 0 \tag{2.29}$$

and

$$h_x = \frac{-1}{(1+a_y{}^2)^{1/2}} \left(\frac{a_t{}^{1/m}}{(1+a_y{}^2)^{1/2m}} D + \theta_s \right), \tag{2.30}$$

where D is the ratio of the velocity scales

$$D = \left(\frac{U}{k} \right)^{1/m} \frac{l}{h_\infty} \tag{2.31}$$

and θ_s the scaled static contact angle

$$\theta_s = \frac{l}{h_\infty} \hat{\theta}_s . \tag{2.32}$$

The parameter D measures the mobility of the contact angle. The value $D = 0$ corresponds to a fixed contact angle.

The boundary conditions far upstream of the contact angle, $x \to -\infty$, are:

$$h = 1, \tag{2.33}$$

plus the condition that all derivatives of h vanish as $x \to -\infty$.

With the above definitions, the leading-order thermal, pressure and velocity fields can be obtained from the shape of the interface h:

$$T(x,y,z,t) = \frac{-Biz}{1+Bih}, \tag{2.34}$$

$$p(x,y,z,t) = G(h-z) - \nabla^2 h, \tag{2.35}$$

$$u(x,y,z,t) = 3\left(\frac{-z^2}{2} + zh + \lambda \right) \left((\nabla^2 h)_x - Gh_x + \frac{1}{1+3\lambda} \right) + \left(z + \frac{\lambda}{h} \right) 2M\Psi(h)\, h_x, \tag{2.36}$$

$$v(x,y,z,t) = 3\left(\frac{-z^2}{2} + zh + \lambda \right) \left((\nabla^2 h)_y - Gh_y \right) + \left(z + \frac{\lambda}{h} \right) 2M\Psi(h)\, h_y, \tag{2.37}$$

$$w(x,y,z,t) = -\int^z (u_x + v_y)\, dz. \tag{2.38}$$

The assumptions about slip, (2.6) and (2.7), and the dependence of surface tension on temperature in the form (2.11) make all the variables well-behaved functions, even at the contact line. In particular, the form of $\Psi(h)$ gives bounded velocities at $x = a(y,t)$, something that the limit $A \to \infty$, i.e. a linear relation, cannot acomplish.

3. Steady state

We begin our analysis of the nonlinear evolution equation (2.22) by looking for steady-state solutions which move down the inclined plane at a constant velocity and have no spanwise variation. In the isothermal case this profile will be determined by a balance between gravity, surface tension and viscous forces. In the non-isothermal case, we also have thermocapillarity effects. Once computed, we will determine the linear stability of this steady-state solution.

The steady-state film thickness, h_0, is determined by looking for solutions independent of y in the system (2.22), (2.29)–(2.33) and by translating the origin to the contact line, $x = a_0(t)$:

$$a(y,t) \to a_0(t), \quad h(x,y,t) \to h_0(\xi) \tag{3.1}$$

$$\xi = x - a_0(t), \quad \tau = t. \tag{3.2}$$

Introducing (3.1) and (3.2) in the system (2.22)–(2.23), integrating once and applying condition (2.29), we find that the steady-state interface shape is determined by

$$-\dot{a}_0 h_0 + \left(h_0^3 + 3\lambda h_0\right)\left(h_0''' - G h_0' + \frac{1}{1+3\lambda}\right) + M\,\Psi(h_0)\,(h_0^2 + 2\lambda)\,h_0' = 0, \tag{3.3}$$

where the prime denotes differentiation with respect to ξ and the overdot differentiation with respect to time. The boundary conditions are

$$h_0(0) = 0, \tag{3.4a}$$

$$h_0'(0) = -\left(\theta_s + D\,\dot{a}_0^{1/m}\right), \tag{3.4b}$$

$$h_0(\xi \to -\infty) = 1, \tag{3.4c}$$

along with the condition that the derivatives of h_0 vanish as $\xi \to -\infty$. Taking the limit $\xi \to -\infty$ in (3.3) and using (3.4c) implies that $\dot{a}_0 = 1$.

The system (3.3)–(3.4) determines the steady-state profile. We note that it is independent of the value of the exponent m appearing in equation (2.15). The contact angle θ is the sum of a static contact angle θ_s and D. Before solving (3.3)–(3.4) numerically, we wish to make some observations about the behaviour of the steady-state solution. First, consider the solution far upstream where $h_0 \to 1$. We linearize (3.3) about the upstream solution $h_0 = 1$ and look for solutions of the resulting third-order linear equation in the form $\exp(r\xi)$. It is easy to show that r is a root of the cubic equation

$$r^3 + 3pr + 2q = 0 \tag{3.5a}$$

where

$$3p = \frac{M(1+2\lambda)\Psi(1)}{1+3\lambda} - G \tag{3.5b}$$

and

$$q = \frac{1}{(1+3\lambda)^2}. \tag{3.5c}$$

Since $q > 0$, one of the roots, r_1, is real and negative and must be discarded. The remaining roots r_2 and r_3 depend on the sign of

$$d = \frac{1}{(1+3\lambda)^4} + \frac{1}{27}\left(\frac{M(1+2\lambda)\Psi(1)}{1+3\lambda} - G\right)^3. \tag{3.6}$$

For the case where $d > 0$, r_2 and r_3, are complex conjugates with positive real part:

$$r_{[2,3]} = \frac{1}{2}\left\{\left[q + d^{1/2}\right]^{1/3} + \left[q - d^{1/2}\right]^{1/3}\right\} \pm \frac{i\sqrt{3}}{2}\left\{\left[q + d^{1/2}\right]^{1/3} - \left[q - d^{1/2}\right]^{1/3}\right\}, \tag{3.7}$$

resulting in the exponential, oscillatory decay of the solution:

$$h_0 = 1 + \{C \exp\{r_2\xi\} + \text{c.c.}\}, \qquad \xi \to -\infty, \tag{3.8}$$

where c.c. denotes complex conjugate and C is a complex constant. As we decrease the angle α that the plate makes with the horizontal, the parameter G increases and eventually d will be negative. In this case all of the roots of (3.5) are real, and again only two of them are positive:

$$r_{[2,3]} = 2|p|^{1/2} \cos\left[\frac{\varphi}{3}, \frac{\pi+\varphi}{3}\right], \tag{3.9a}$$

where

$$\cos\varphi = \frac{-q}{|p|^{3/2}}. \tag{3.9b}$$

In this case, there is no oscillatory behaviour of the far-field decaying solution:

$$h_0 = 1 + C_2 \exp\{r_2\xi\} + C_3 \exp\{r_3\xi\}, \qquad \xi \to -\infty, \tag{3.10}$$

where C_2 and C_3 are real constants.

From this analysis, one can conclude that the far-field solution depends weakly on the small parameter λ. On the other hand, for small p, one of the complex roots of (3.5) is given by

$$r_2 = \left(\frac{q}{4}\right)^{1/3}(1+\mathrm{i}\sqrt{3}) - \left[\left(\frac{1}{432q}\right)^{1/3}(1-\mathrm{i}\sqrt{3})\right] p + O(p^3), \tag{3.11}$$

i.e. as the Marangoni number increases (or G decreases), the wavelength along the interface far upstream decreases, but the undulations are less damped.

Now consider the behaviour of the solution of the nonlinear equation (3.3) in the neighbourhood of the contact line. We look for a solution in the form of a power series in ξ about $\xi = 0$:

$$h_0 = \sum_{n=0}^{\infty} c_n \xi^n. \tag{3.12}$$

Substituting the series (3.12) into (3.3), using the boundary conditions (3.4), and collecting powers of ξ, we obtain the values of the coefficients. In the isothermal case, $M = 0$, these are

$$c_0 = 0, \quad c_1 = -(\theta_s + D), \quad c_3 = \frac{1}{18\lambda(1+3\lambda)} + \frac{Gc_1}{6}, \quad c_4 = \frac{Gc_2}{12} \tag{3.13a}$$

and for $n > 4$

$$c_n = \frac{(n-3)!}{3\lambda n!}\left\{3\lambda G\,(n-2)c_{n-2} - \left(\frac{1}{1+3\lambda}\right)\sum_{j=1}^{n-4} c_j c_{n-j-3} + \sum_{k=2}^{n-3}\left(G\,(n-k-2)\,c_{n-k-2} - \frac{(n-k)!\,c_{n-k}}{(n-k-3)!}\right)\sum_{j=1}^{k-1} c_j c_{k-j}\right\}. \tag{3.13b}$$

Note that the c_n depend on the value of the second derivative at the contact line $h_0''(0) = 2c_2$. This number is the only unknown coefficient in the series solution, and can be determined by matching to the solution away from the contact line. This is a difficult task, but we can do it numerically if necessary. It is important to note that since a solution of the nonlinear equation (3.3) can be found in the form of a power series, then h_0 and all of its derivatives are finite at the contact line. Hence there is no singularity at the contact line. This result is due to the form of the slip function

(2.7) we have chosen. A constant slip function would have led to a singularity in the second derivative. A similar observation has been noted for the initial motion of a droplet by Haley & Miksis (1991).

In the non-isothermal case when $M \neq 0$ extra terms must be added to the coefficients in (3.13). The exact values can be found in the Appendix. Nevertheless, the situation is very similar to the isothermal case: h_0 and all of its derivatives are finite at the contact line. This is a direct consequence of equation (2.11).

In order to understand the steady-state solution, we need to solve the nonlinear equation (3.3) numerically. This is done by using a Chebyshev pseudo-spectral approximation of the derivatives (Canuto *et al.* 1988), and then forcing the boundary conditions (3.4) at the contact line $\xi = 0$ and at the end of the computational domain $\xi = -L$. The computational domain is given by $-L \leqslant \xi \leqslant 0$ and L is chosen sufficiently large in order to simulate the correct boundary condition, which should be imposed at negative infinity. For the calculations presented here, setting $L = 20$ seemed to give accurate results. In addition, at $\xi = -L$, we set the first derivative of h_0 to zero. The result of this discretization is a nonlinear system of equations for the values of h_0 at the collocation points. This system was solved by using Newton's method.

Although the specific value of the slip coefficient is unknown, we expect it to be small. As shown in Haley & Miksis (1991) in their study of droplet spreading, the magnitude of the slip coefficient affects the quantitative behaviour of the contact line motion, but not the qualitative behaviour. However, as can be seen from the coefficients (3.13) in the power series expansion about the contact line, as λ decreases the magnitudes of the derivatives increase. Hence, the smaller the λ, the larger the number of collocation points we need in the neighbourhood of the contact line in order to resolve the solution. We have set $\lambda = 0.001$ in all of the results presented here. This number does not appear to give results much different than for smaller values of λ, while it allows for a reasonable number of collocation points in our calculations.

We begin our study of the steady-state profiles with the isothermal case, $M = 0$. In figure 3 we plot the steady-state film thickness as a function of ξ, for $\theta_s = 0.6, D = 1$ and $G = 0, 1.5, 2.5, 4$. As G increases, the pressure in the interface grows, and the interface gets smoother. As shown in figure 3, the amplitude of the initial hump decreases with increasing G, while its width increases, as implied by the far-field analysis. For small values of G, this behaviour was predicted by equation (3.11) to be linear in G. On the other hand, for $G > 3/(1+3\lambda)^{2/3}$ the upstream oscillatory behaviour is lost ($G = 4$ in figure 3).

Continuing with our investigation of the isothermal case, $M = 0$, in figure 4 we plot the steady-state film thickness for $G = 1.0$ and different values of the contact angle: $\theta = D + \theta_s = 0.61, 1.6, 3.1, 4.1$. This quantity only appears in the boundary condition for the derivative of the steady state at the contact line (3.4). The value of θ does not affect the value of the upstream solution, but the derivative at the contact line changes with θ. In figure 4, we show how the height of the hump increases with the contact angle θ.

Consider now the heated case. In equation (3.3) M, A and Bi appear as parameters and if $Bi = 0$, then one should also set M and A equal to zero. Nevertheless, we will first ignore the heat transfer coefficient Bi. As discussed in Ehrhard & Davis (1991), this is still a reasonable limit to consider because even with a quasi-static temperature profile a growing wave has variations in its crest and trough surface temperatures. This is a possible mechanism of thermocapillarity instabilities along

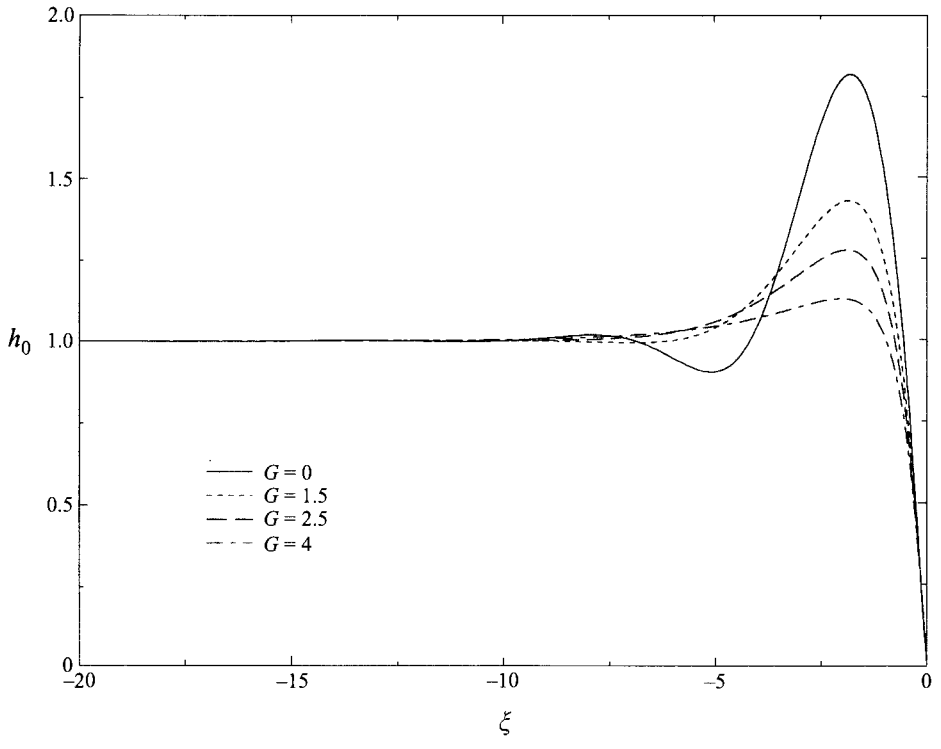

FIGURE 3. Steady state for different values of the parameter G with $\theta_s = 0.6$, $D = 1$, $\lambda = 0.001$ and no heat transfer, i.e. $M = 0$.

the interface. In figure 5 we plot the film thickness for $G = 1.0$, $D + \theta_s = 1.6$, $A = 1.0$ and $M = 0, 1, 2, 2.5$. We find that, as M increases, the height of the hump increases and the wavelength of the oscillations decreases upstream. The latter observation is consistent with the linear analysis estimate of the behaviour of the interface far upstream. The Marangoni number M opposes the smoothing caused by increasing the parameter G. For the values considered here, we have the oscillatory decaying case, equations (3.7) and (3.8). In particular, we find that the real part of the complex root, m_2, decreases as M increases from zero, i.e. the exponential damping decreases with increasing M. The magnitude of the imaginary part increases and the wavelength of the far-field oscillations decreases with the Marangoni number. One would expect this result because of the appearance of tangential stresses in the liquid–gas interface as a result of surface tension gradients due to the heating. The Marangoni number does not modify the value of the contact angle, and only affects higher derivatives. In figure 6 we keep the same parameter values as in figure 5, except $M = 1$ is fixed and $Bi = 0$, 0.2, 0.6, 5.0. The Biot number does not modify the value of the contact angle. As we increase its value from the adiabatic limit $Bi = 0$, more energy is dissipated at the interface and this decreases the height of the hump. It also increases the wavelength of the upstream surface oscillations. Hence surface heat transfer tends to inhibit thermocapillary effects and makes the surface smoother.

The effect of the parameter A on the solution is shown in figure 7. For $G = 1, \theta_s = 1.6$ and $Bi = 0$ fixed, we consider two different values of the Marangoni number, $M = 1$ and $M = 2$, and in each case we set $A = 1$ and $A = 5$. When $A = 0$, ($\Psi(h_0) = 0$), there are no surface tension variations and consequently no

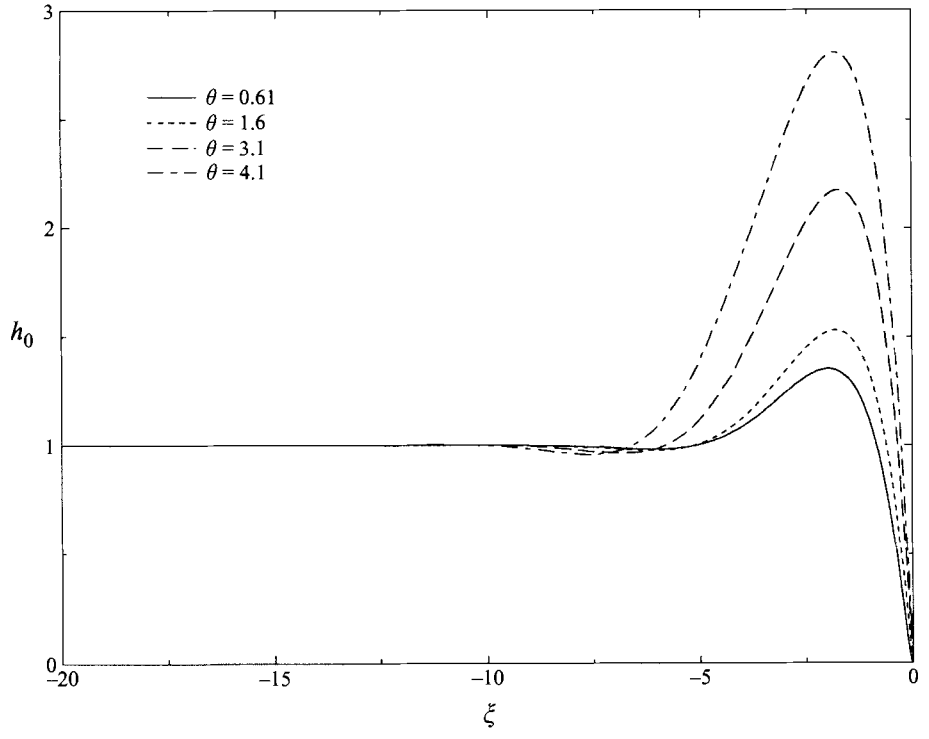

FIGURE 4. Steady state for different values of the contact angle $\theta = D + \theta_s$, with $G = 1, \lambda = 0.001$ and no heat transfer, i.e. $M = 0$.

heating effects. When A increases, the exponential term in the function $\Psi(h_0)$ is designed to have little effect on the far-field solution; in fact, $\Psi(1)$ has a maximum value when $A = 2$ and $\Psi(1) = 1$ as $A \to \infty$. Nevertheless, the Marangoni effects increase a little as shown in figure 7. Like M, the parameter A only affects the higher derivatives at the contact line (see Appendix).

4. Linear stability

Our aim here is to determine the linear stability of the basic state h_0 which was determined numerically in the previous section. Let the free surface $h(x, y, t)$ and the leading edge $a(y, t)$ suffer small increments from their steady values $h_0(\xi)$ and $a_0(t)$. We obtain the equations for the perturbations by neglecting powers of δ higher than the first when we substitute into equation (2.22) the dependent variables

$$a(y,t) \to a_0(t) + \delta \exp\{\sigma t + iqy\}, \tag{4.1}$$

$$h(x,y,t) \to h_0(\xi) + \delta h_1(\xi) \exp\{\sigma t + iqy\}. \tag{4.2}$$

Here the perturbations have been expressed in terms of normal modes. The resulting linear equation is

$$A_4(h_0)h_1'''' + A_3(h_0)h_1''' + A_2(h_0)h_1'' + A_1(h_0)h_1' + A_0(h_0)h_1 = -\sigma h_1 \tag{4.3a}$$

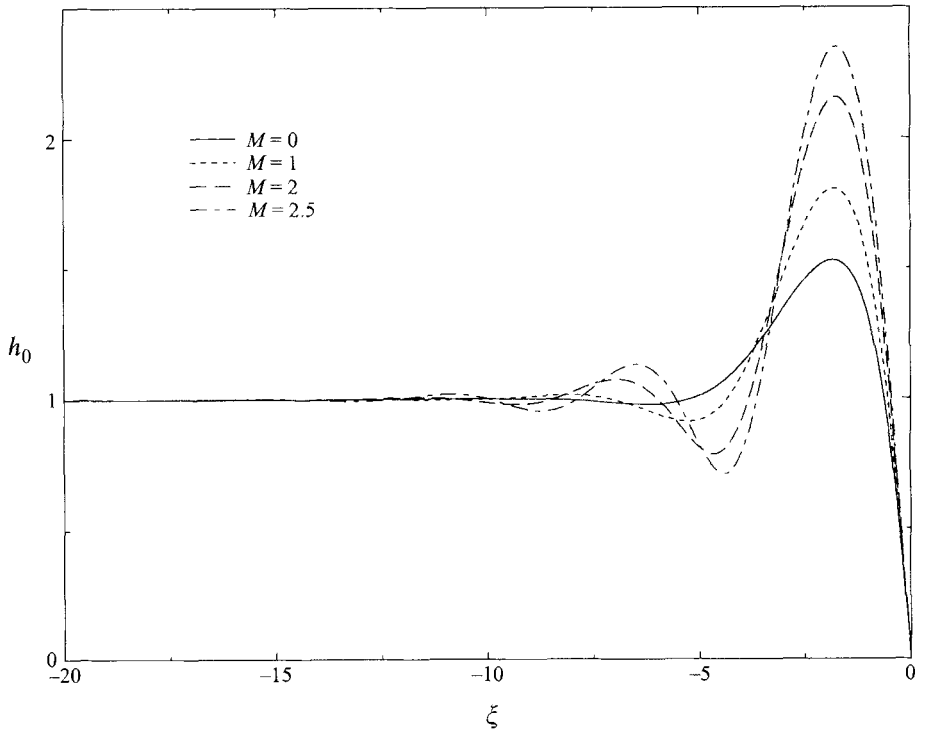

FIGURE 5. Steady state for different values of the Marangoni number M, with $G = 1$, $\theta_s = 0.6$, $D = 1$, $\lambda = 0.001$, $A = 1$ and no heat flux in the free surface, i.e. $Bi = 0$.

where the coefficients A_i are given by

$$\left.\begin{aligned}
A_4(h_0) &= \left(h_0^3 + 3\lambda h_0\right), \\
A_3(h_0) &= 3\left(h_0^2 + \lambda\right) h_0', \\
A_2(h_0) &= M\left(h_0^2 + 2\lambda\right) \Psi(h_0) - A_4\left(G + 2q^2\right), \\
A_1(h_0) &= 3\left(h_0^2 + \lambda\right)\left(h_0''' + \frac{1}{1+3\lambda}\right) - 1 + 2M\left[\left(h_0^2 + 2\lambda\right) \Psi(h_0)\right]' - A_3\left(G + 2q^2\right), \\
A_0(h_0) &= 3\left[\left(h_0^2 + \lambda\right)\left(h_0''' + \frac{1}{1+3\lambda}\right)\right]' + M\left[\left(h_0^2 + 2\lambda\right) \Psi(h_0)\right]'' - q^2 A_2 .
\end{aligned}\right\} \tag{4.3b}$$

The corresponding boundary conditions for the linear problem are

$$h_1(0) = -h_0'(0) = \theta_s + D, \qquad h_1'(0) = -h_0''(0) - \frac{D}{m}\sigma, \qquad h_1(\xi \to -\infty) = 0, \tag{4.4}$$

and the derivatives of h_1 vanish as $\xi \to -\infty$.

For every value of the wavenumber q, we obtain an eigenvalue problem for the growth rate σ. We look for complex eigenvalues σ with the physical parameters fixed, and assign a value to the wavenumber q. This is done numerically, using a Chebyshev spectral method to discretize the derivatives. The eigenvalues of the real matrix associated with the discrete problem are found using the routine 'hqr' from Eispack for real upper Hessenberg matrices (Smith 1982). In all of the cases we have considered, the eigenvalue with the largest real part was found to have

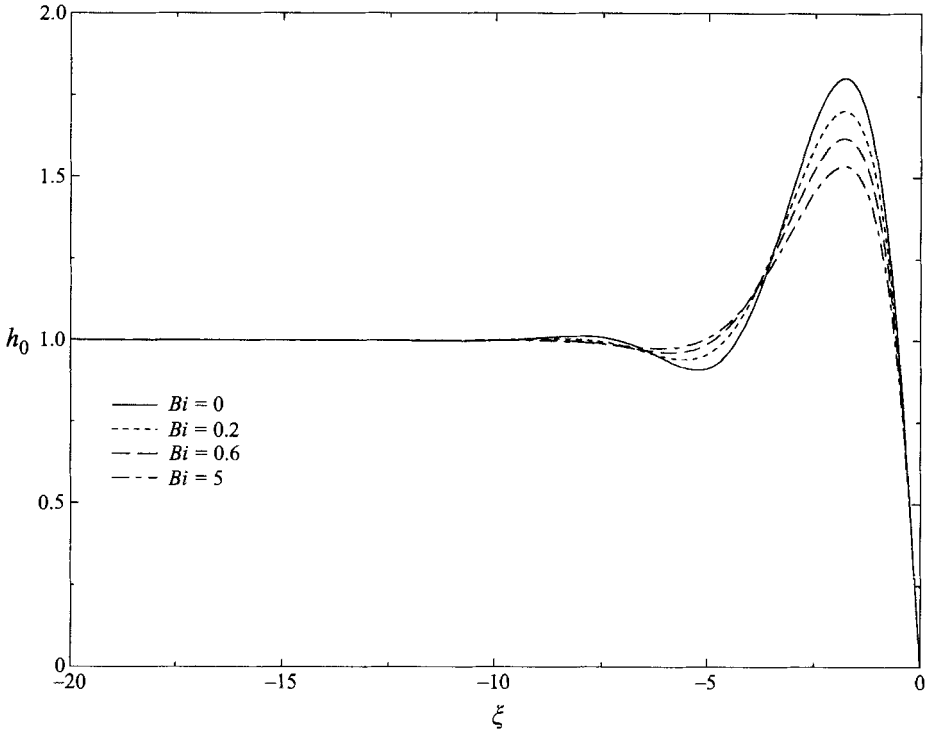

FIGURE 6. Steady state for different values of the Biot number Bi, with $G = 1$, $\theta_s = 0.6$, $D = 1$, $\lambda = 0.001$, $M = 1$ and $A = 1$.

$\mathrm{Im}\{\sigma\} = 0$, i.e. the fastest-growing mode is purely real. This implies that one could have looked only for real eigenvalues. In the following, we present results only for the eigenvalue σ with the largest real part. Typical curves are shown in figure 8, where the real eigenvalue σ is given as a function of the wavenumber q. In particular, for $q = 0$ the eigenvalue with the largest real part is $\sigma = 0$ and the correponding eigenfunction is $h_1(x) = -h_0'(x)$. This can be shown by simple substitution into equations (4.3) and (4.4). As q increases, σ increases and remains positive, reaches a maximum σ_{max} at $q = q_{max}$, then decreases with increasing q and becomes zero at $q = q_b$. For $q > q_b$ all the eigenvalues have negative real part. Hence the steady state is unstable for values of q between 0 and q_b, the upper boundary of the unstable wavenumbers. In figure 8 we have considered four different cases with $m = 3$, $D = 1.0$, $\lambda = 0.001$, $\theta_s = 0.6$, $A = 1$ and $Bi = 0$. In the first, we have set $G = 0$, $M = 0$, i.e. no heat transfer and a vertical wall. Then we decrease the plate angle, such that $G = 2.5$. We see that as a result, q_{max}, q_b and σ_{max} decreased with G. Next we fix $G = 1$ and include thermocapillary effects by putting $M = 0.5$ and $M = 1$. Now, q_{max}, q_b and σ_{max} increased with M. Clearly from figure 8 we see that the important features of the curves are σ_{max}, the corresponding value of $q = q_{max}$ and the value of q_b. The value of q_b bounds the range of unstable wave-numbers, while σ_{max} and q_{max} specify the expected observable growth rate and corresponding wave-number. In order to understand the effect of all the parameters on the linear stability of the film, in the following we will show how these three variables depend on the physical parameters G, θ_s, D, M, Bi and A. In all cases, we will take $m = 3$ in the slip velocity versus contact angle relationship. This value seems to give good

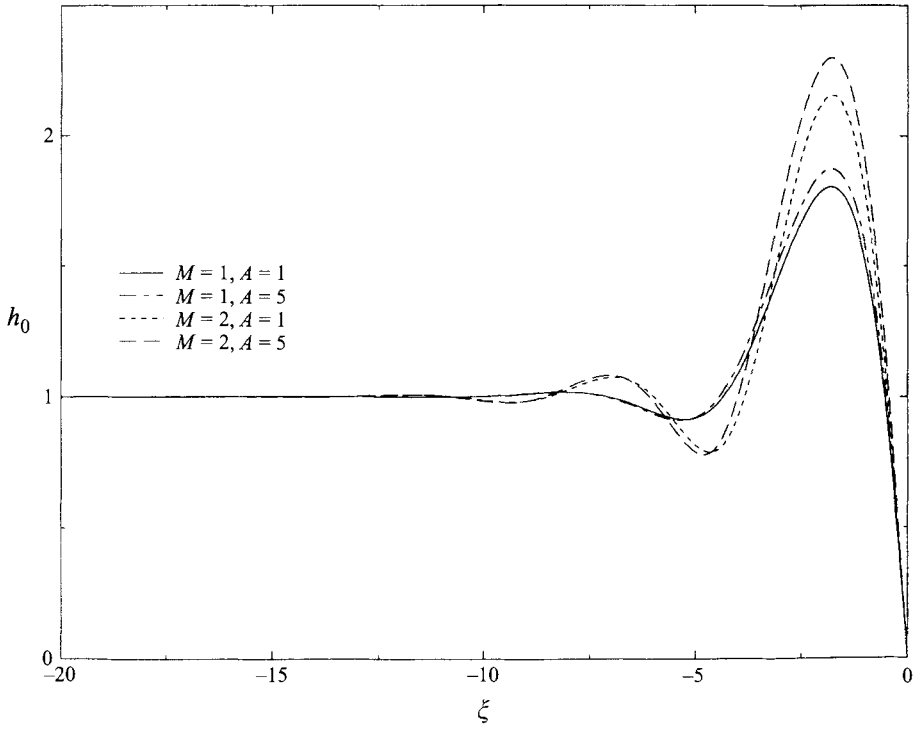

FIGURE 7. Steady state for $A = 1$ and $A = 5$, with $G = 1$, $\theta_s = 0.6$, $D = 1$, $\lambda = 0.001$ and $Bi = 0$. In each case we consider two different values of the Marangoni number: $M = 1$ and $M = 2$.

agreement with experiment in the drop spreading problem studied by Ehrhard & Davis (1991).

Figure 9(*a*) shows q_{max} and q_b as functions of the parameter G, with $D = 1$, $\theta_s = 0.6$, $\lambda = 0.001$ and no heat transfer, $M = 0$. We see that both q_{max} and q_b are decreasing functions of G. Since the q_b curve represents values of q which are neutrally stable, all values of q below the curve are unstable, while values above the curve are stable. The value $G = 0$ corresponds to a vertical wall. As G increases, the pressure drop across the depth of the fluid increases relative to the normal stresses and we expect the interface to be more stable, as shown in the figure. In figure 9(*b*) we plot the corresponding values of σ_{max} as a function of G. The maximum growth rate σ_{max} decreases with increasing G. This means that perturbations in the spanwise direction will grow more slowly with increasing G, which is a plausible result. The steady-state solutions presented in figure 3 for different values of G show that as the parameter G increases, the initial hump decreases, and the solution gradually loses its oscillatory behaviour when the effect of the vertical pressure gradients is larger than the driving force. This is roughly represented by $d < 0$ in equation (3.6). The changes in q_b, q_{max} and σ_{max} are large for the range of G studied here, but large values of G correspond to very low inclination angles, since $Ca^{1/3}$ is buried in the definition of G, equation (2.24). The linear stability analysis of Troian *et. al.* (1989) for the precursor film model and large inclination angles gives $q_{max} \approx 0.45$ and $q_b \approx 0.9$. These values are comparable with the values for $G = 0$, where $q_{max} = 0.482$ and $q_b = 0.825$.

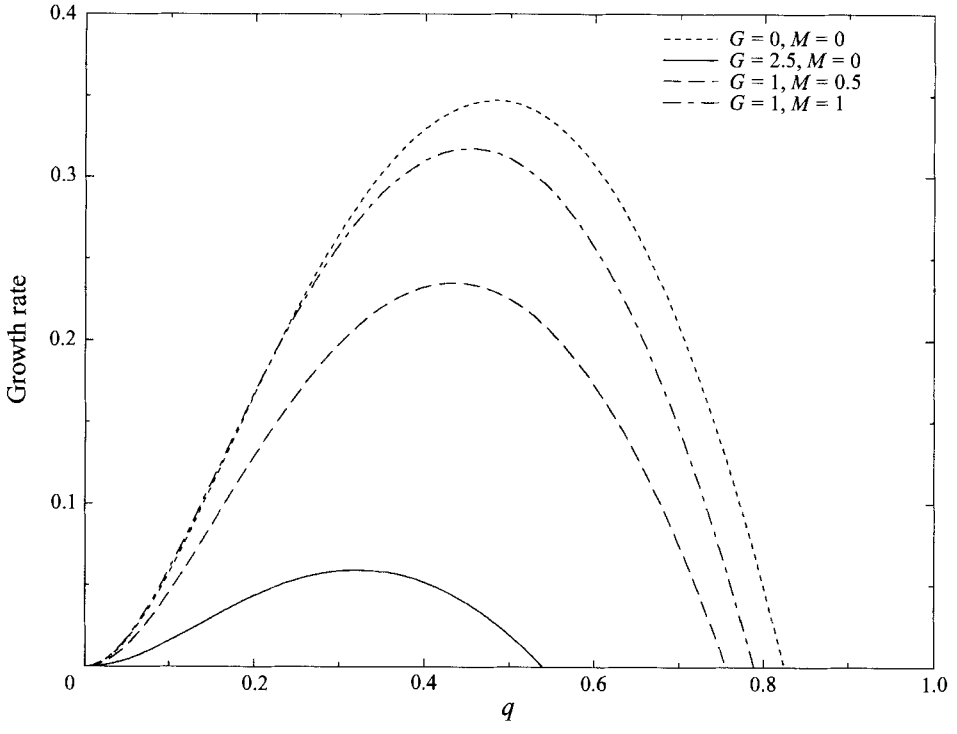

FIGURE 8. The growth rate σ as a function of the wavenumber q, for different values of the parameter G and the Marangoni number M, with $\theta_s = 0.6$, $D = 1$, $\lambda = 0.001$, $Bi = 0$ and $A = 1$.

The solution is affected by both the static contact angle θ_s and the dynamic contact angle, the latter controlled by the parameter D. In the case of a time-independent straight leading edge we had to deal only with the total value of the contact angle $\theta = \theta_s + D$, but now we must treat them as separate quantities. Suppose we fix $\lambda = 0.001$, $G = 1$, $M = Bi = 0$ and set $D = 1$, while we let θ_s vary. As shown in figure 10(a), the behaviour of q_{max} and q_b with θ_s is non-monotonic. On the other hand, from figure 10(b) one sees that the changes in σ_{max} are relatively faster with increasing θ_s, particularly at larger values of θ_s.

We proceed by taking $\theta_s = 0.6$ fixed, while the values of the other parameters remain the same, and perform a linear analysis as a function of the ratio of velocity scales D. In figure 11(a), q_b and q_{max} are plotted as functions of the parameter D. We again find a region of slowly growing q_b and q_{max} with D. As this parameter becomes larger the front becomes more stable with increasing D. The maximum value of q_b and q_m as functions of θ_s and D are very similar. Figure 11(b) shows the dependence of σ_{max} on D. As D grows from $D = 0$ (the fixed contact angle case), the perturbations initially grow, then reach a maximum value of σ_{max}, after which σ_{max} decreases very slowly.

The effects of temperature differences are represented by the Marangoni number M. We set $G = 1.0$, $\theta_s = 0.6$, $D = 1$, $A = 1$ and $Bi = 0$, and plot the values of q_{max} and q_b as functions of M in figure 12(a). We find that for small M, q_{max} and q_b increase with increasing M. Recall from figure 9(a) that these wavenumbers decreased with the parameter G. This inverse behaviour is the same as for the oscillatory instabilities in the x-direction when we studied the steady solutions, where the hump in the steady-state profiles of figure 5 increases in amplitude and narrows with increasing

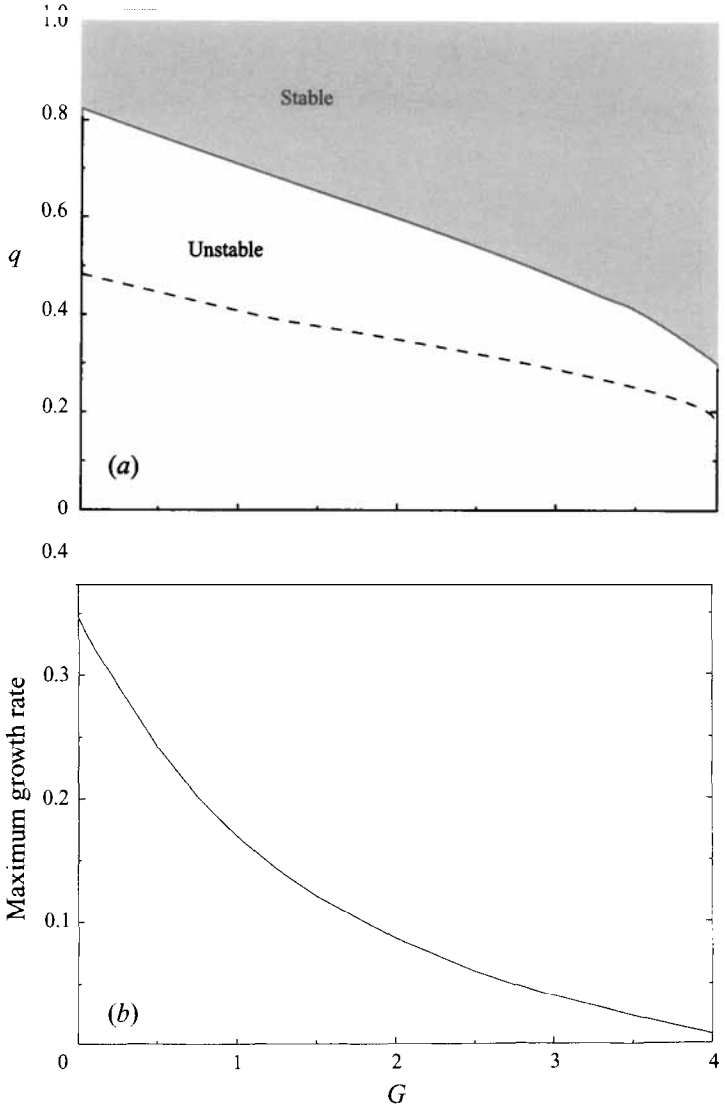

FIGURE 9. Linear stability analysis for the parameter G, with $\theta_s = 0.6$, $D = 1$, $\lambda = 0.001$ and no heat transfer. (*a*) Marginal stability wavenumber q_b (——) and wavenumber for maximum growth rate q_{max} (— — —) as functions of the parameter G. (*b*) Maximum growth rate σ_{max} as a function of the parameter G.

M. We conclude that for small M, heating has a destabilizing effect. For large values of M the curves for q_{max} and q_b attain a maximum around $M = 2$ and then decrease. Hence, for large M thermocapillary effects could be a stabilizing factor for the spanwise perturbations. Similar behaviour is found when for σ_{max} as a function of M. For $M \approx 2$ we reach a maximum for σ_{max}, which then decreases (figure 12*b*).

The instability produced by the Marangoni effect can be reduced by allowing more heat to dissipate at the liquid-gas interface, as shown in figures 13(*a*) and 13(*b*). Here we allow the Biot number Bi to vary and plot q_{max}, σ_{max} and q_b. We set $M = 1$, and the other parameters as in figure 12(*a*). Now we find that q_{max}, σ_{max} and q_b all decrease with increasing Bi, implying improved stability when we increase the dimensionless

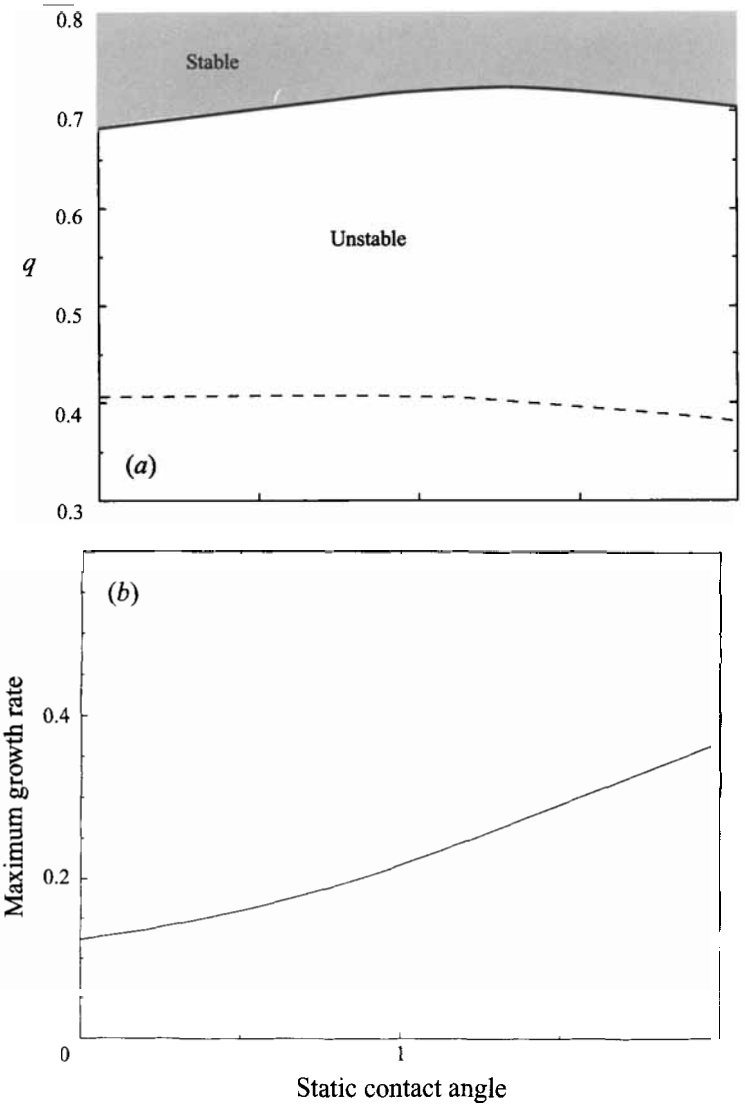

FIGURE 10. Linear stability analysis for the static contact angle θ_s, with $G = 1$, $D = 1$, $\lambda = 0.001$ and no heat transfer. (*a*) Marginal stability wavenumber q_b (——) and wavenumber for maximum growth rate q_{max} (— — —) as functions of the static contact angle. (*b*) Maximum growth rate σ_{max} as a function of the static contact angle.

heat transfer coefficient. In figures 13(*a*) and 13(*b*) as $Bi \to \infty$ we recover the values without heat transfer.

With this background, we wish to determine how much the assumption made for the surface tension variations with temperature, (equation (2.11)) affects the linear analysis. We plot q_{max} and q_b for $G = 1.0$, $\theta_s = 0.6$, $D = 1.0$, $\lambda = 0.001$ $M = 1.0$ and $Bi = 0$ in figure 14(*a*). For $A = 0$ no heating is present. As A increases the values of q_{max} and q_b increase rapidly up to $A = 1$. After that their value decreases very slowly with A. In figure 14(*b*) we plot σ_{max} as a function of A. Again we see a region of rapid change, where σ_{max} grows but as this parameter gets large, this growth is very slow.

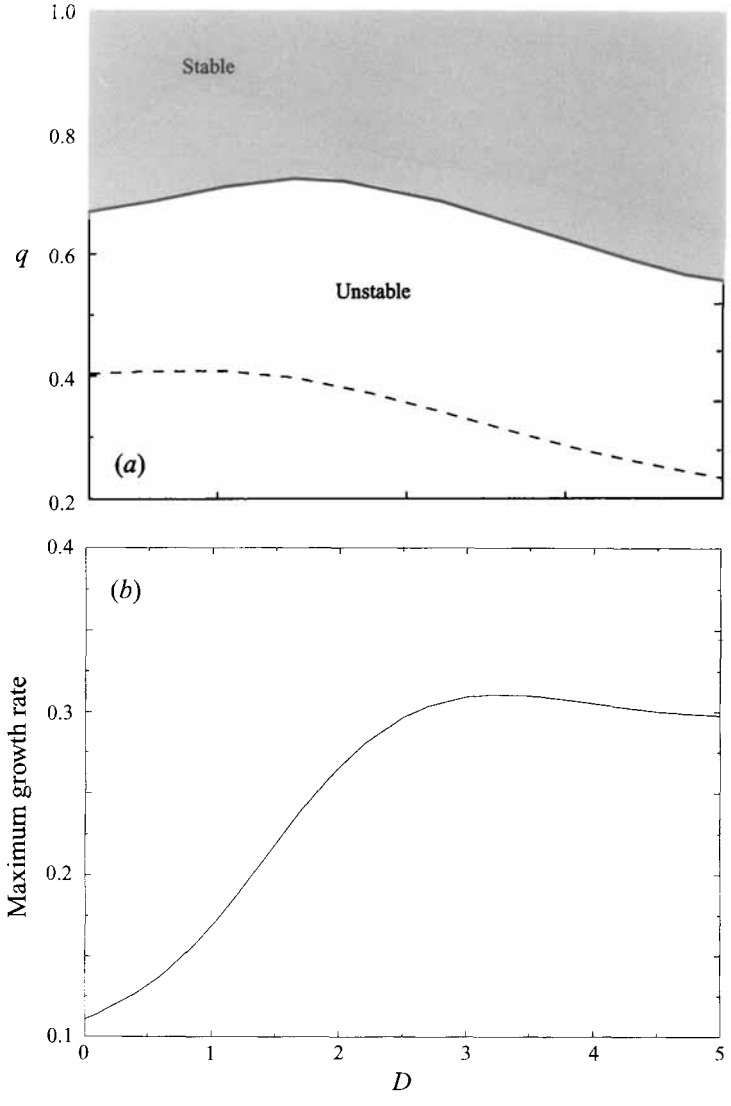

FIGURE 11. Linear stability analysis for the parameter D, with $G = 1$, $\theta_s = 0.6$, $\lambda = 0.001$ and no heat transfer. (*a*) Marginal stability wavenumber q_b (——) and wavenumber for maximum growth rate q_{max} (— — —) as functions of the parameter D. (*b*) Maximum growth rate σ_{max} as a function of the parameter D.

5. Conclusions

We have determined the steady-state profile for a thin, non-isothermal coating film flowing down an inclined plane. In addition, we have studied the linear stability of this film to spanwise disturbances. Both the steady-state and the linear disturbance equations were solved numerically. It has been shown that, if in the isothermal case a singular slip coefficient (2.7) is used in the Navier slip condition (2.6), then the steady-state solution is regular in the neighbourhood of the contact line. This was done by determining the power series solution about the contact line. This implies that a numerical solution can be determined without a special analysis about the contact point. If a constant slip coefficient had been used in equation (2.6), singularities in

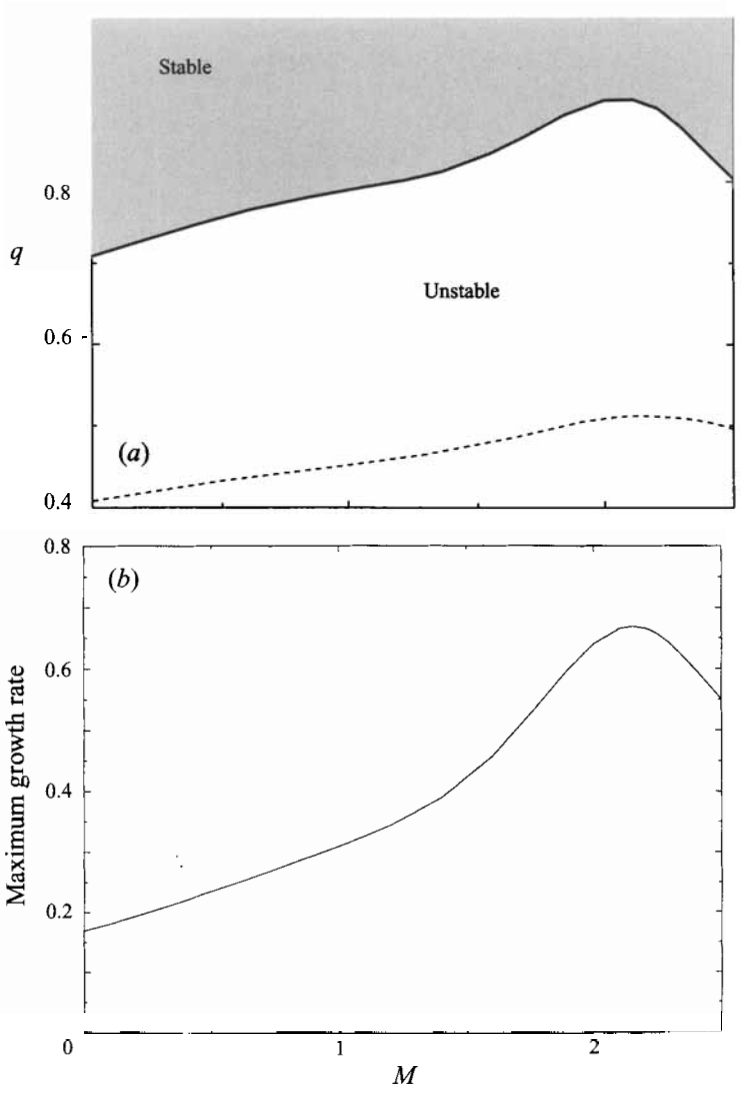

FIGURE 12. Linear stability analysis for the Marangoni number, with $G = 1$, $\lambda = 0.001$, $D = 1$, $A = 1$ and $Bi = 0$. (*a*) Marginal stability wavenumber q_b (——) and wavenumber for maximum growth rate q_{max} (— — —) as functions of the Marangoni number. (*b*) Maximum growth rate σ_{max} as a function of the Marangoni number.

the interface $h_0(x)$ would be expected in the second derivative at the contact point in the isothermal case (Haley & Miksis 1991). In the heated case, we also find for our model that the interface is a regular function at the contact line.

We retained the term representing vertical pressure gradients in our model and showed that in general it has a stabilizing effect on the interface. The steady solutions are shown to have a contact angle composed of a static part and a term due to the dynamics. This contact angle tends to increase the height of the hump present in the solution. Static contact angles or large variations in the dynamic contact angle have a non-monotonic behaviour in the stability analysis for perturbations in the direction

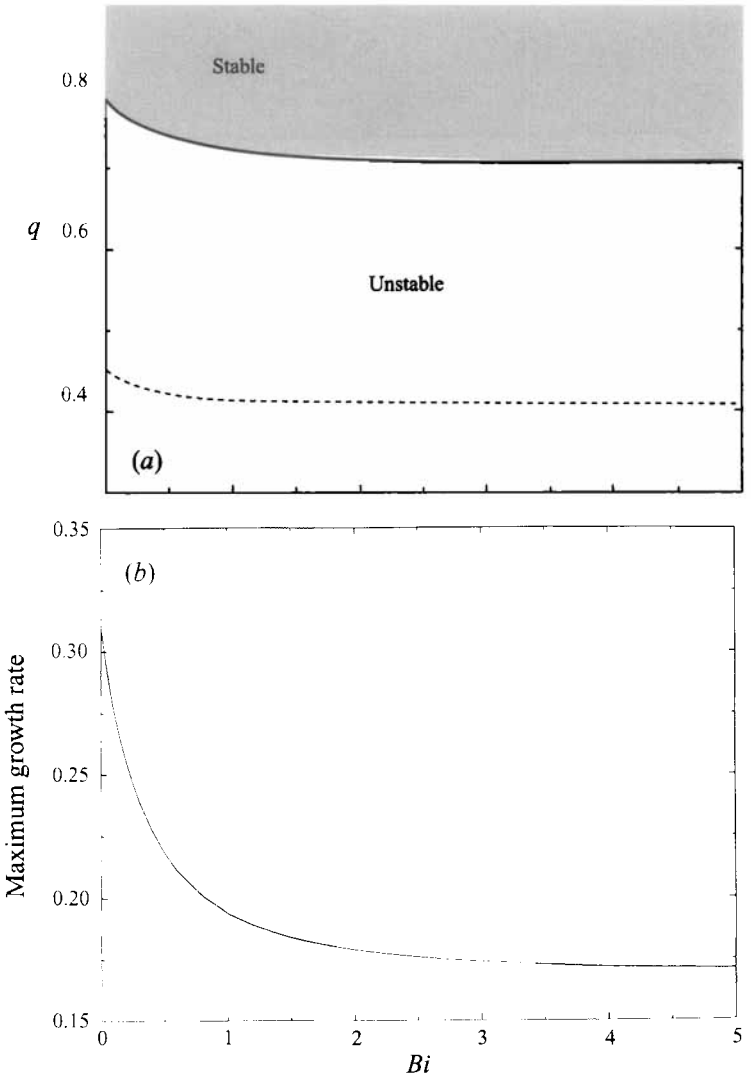

FIGURE 13. Linear stability analysis for the Biot number, with $G = 1$, $\theta_s = 0.6$, $D = 1$, $M = 1$ and $A = 1$. (*a*) Marginal stability wavenumber q_b (——) and wavenumber for maximum growth rate q_{max} (— — —) as functions of the Biot number. (*b*) Maximum growth rate σ_{max} as a function of the Biot number.

perpendicular to the flow. Both quantities have a very slow destabilizing effect for small values, but they have the contrary effect for large values.

The perturbed steady-state solutions showed that heating the plate produces oscillations that grow in amplitude and wavenumber in the downstream direction. This is in accord with the general observations of destabilization (stabilization) by thermocapillary effects (Burelbach *et al.* 1988 and Joo *et al.* 1991) of continuous films on a heated (cooled) wall. Physically, for films on a heated wall, the troughs are hotter than the crests. Since surface tension in nearly all cases decreases monotonically with increasing temperature, this draws liquid towards the crests, resulting in further growth of the crests. Meanwhile, small heating causes a destabilizing effect

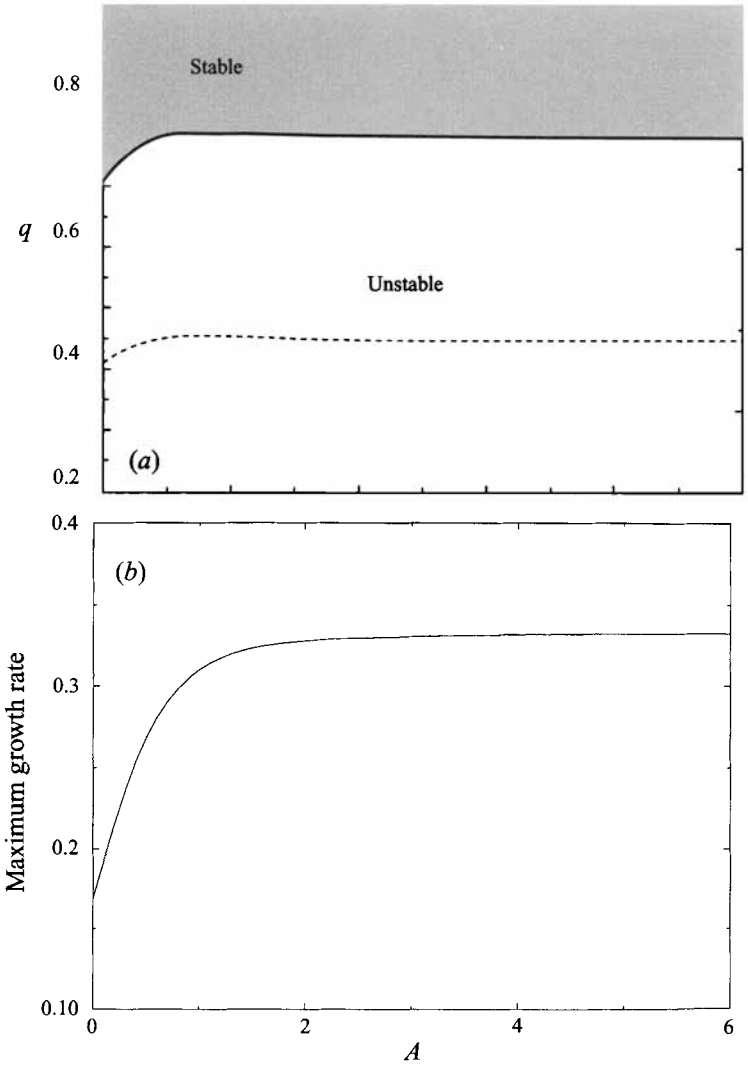

FIGURE 14. Linear stability analysis for the parameter A, with $G = 1$, $\theta_s = 0.6$, $D = 1$, $M = 1$ and $Bi = 0$. (*a*) Marginal stability wavenumber q_b (———) and wavenumber for maximum growth rate q_{max} (— — —) as functions of the parameter A. (*b*) Maximum growth rate σ_{max} as a function of the parameter A.

in the leading front of a coating film. In particular, small heating increases the band of unstable wavenumbers and the growth rate of the most unstable wavenumbers. For large temperature gradients, the heating could be a stabilizing effect. This non-monotonic behaviour is similar to the one found for the contact angle and contact angle variations, which suggests that increasing the hump in the steady-state solution could be responsible for these phenomena. On the other hand, increasing the Biot number and allowing more heat to dissipate at the liquid–gas interface inhibits the effect of the heating.

Acknowledgement

This research was supported in part by NSF Grant No. CTS-9223464. The authors wish to thank the referees for several very helpful comments.

Appendix

We substitute the power series in ξ:

$$h_0 = \sum_{n=0}^{\infty} c_n \xi^n, \tag{A1}$$

into the complete steady-state equation (3.3) and look for the coefficients in the complete equation. As before, we use the boundary conditions at the contact line and collect powers of ξ, to obtain the coefficients

$$c_0 = 0, \qquad c_1 = -(\theta_s + D),$$

$$c_3 = \frac{1}{18\lambda(1+3\lambda)} + \frac{G c_1}{6} - \frac{2MA c_1}{9},$$

$$c_4 = \frac{G c_2}{12} + \frac{MA}{72}\left\{3(A+4Bi)\, c_1^2 - 8c_2\right\},$$

and for $n > 4$

$$c_n = \frac{(n-3)!}{3\lambda n!}\left\{3\lambda G(n-2)c_{n-2} - \left(\frac{1}{1+3\lambda}\right)\sum_{j=1}^{n-4} c_j c_{n-j-3} + \sum_{k=2}^{n-3}\left[\left(G(n-k-2)\, c_{n-k-2} - \frac{(n-k)!\, c_{n-k}}{(n-k-3)!}\right)\sum_{j=1}^{k-1} c_j c_{k-j}\right] - M\sum_{j=0}^{n-3}\left[\frac{(n-j-2)c_{n-j-2}}{j!}\left(\frac{\mathrm{d}^j F_0}{\mathrm{d}\xi^j}\Big|_{\xi=0}\right)\right]\right\}, \tag{A2}$$

where the jth derivative of the function

$$F_0 = \frac{(h_0(\xi)^2 + 3\lambda)\,\Psi(h_0(\xi))}{h_0(\xi)} \tag{A3}$$

must be calculated applying the chain rule j times. The existence of these derivatives at $\xi = 0$ is a consequence of the equation of state for the surface tension (2.11). Again for $n > 3$, the coefficients in the series depend on c_2.

REFERENCES

Bruyn, J. R. de 1992 Growth of fingers at a driven three-phase contact line. *Phys. Rev.* A **46**, R4500–R4503.

Burelbach, J. P., Bankoff, S. G. & Davis, S. H. 1988 Stability of evaporating condensing liquid films. *J. Fluid Mech.* **195**, 463–494.

Canuto, C., Hussaini, M. Y., Quarteroni, A. & Zang,T. A. 1988 *Spectral Methods in Fluid Dynamics.* Springer.

Cazabat, A. M. 1991 Wetting films. *Adv. Colloid Interface Sci.* **34**, 72–88.

Dussan V., E. B. 1976 The moving contact line: the slip boundary condition. *J. Fluid Mech.* **77**, 665–684.

Dussan V., E. B. 1979 On the spreading of liquids on solid surfaces: Static and dynamic contact lines. *Ann. Rev. Fluid Mech.* **11**, 371–400.

Dussan V., E. B. & Davis, S. H. 1974 On the motion of a fluid–fluid interface along a solid surface. *J. Fluid Mech.* **65**, 71–96.

Ehrhard, P. 1993 Experiments on isothermal and non-isothermal spreading. *J. Fluid Mech.* **257**, 463-483.

Ehrhard, P. & Davis, S. H. 1991 Non-isothermal spreading of liquid drops on horizontal plates. *J. Fluid Mech.* **229**, 365–388.

Gennes, P. G. de 1985 Wetting: statics and dynamics. *Rev. Mod. Phys.* **57**, 828–861.

Goodwin, R. & Homsy, G. M. 1991 Viscous flow down a slope in the vicinity of a contact line. *Phys. Fluids* A **3**, 515–528.

Greenspan, H. P. 1978 On the motion of a small viscous droplet that wets a surface. *J. Fluid Mech.* **84**, 125–143.

Haley, P. J. & Miksis, M. J. 1991 The effect of the contact line on droplet spreading. *J. Fluid Mech.* **223**, 57–81.

Hocking, L. M. 1990 Spreading and instability of a viscous fluid sheet. *J. Fluid Mech.* **211**, 373–392.

Hocking, L. M. 1992 Rival contact-angle models and the spreading of drops. *J. Fluid Mech.* **239**, 671–681.

Hocking, L. M. & Miksis, M. J. 1993 Stability of a ridge of fluid. *J. Fluid Mech.* **247**, 157–177.

Huppert, H. E. 1982 Flow and Instability of viscous gravity currents down a slope. *Nature* **300**, 427–429.

Joo, S. W., Davis, S. H. & Bankoff, S. G. 1991 Long-wave instabilities of heated falling films: two-dimensional theory of uniform layers. *J. Fluid Mech.* **230**, 117–146.

Kelley, R. E., Davis, S. H. & Goussis, D. A. 1986 On the instability of heated film flow with variable surface tension. In *Heat Transfer 1986. Proc. 9th Intl Heat Transfer Conference, San Francisco*, vol. 4, pp. 1936–1942.

Lin, S. P. 1975 Stability of liquid flow down a heated inclined plane. *Lett. Heat Mass. Transfer* **2**, 361–370.

Renk, F., Wayner, P. C. Jr & Homsy, G. M. 1978 On the transition between a wetting film and a capillary meniscus. *J. Colloid Interface Sci.* **67**, 408–414.

Schwartz, A. M. & Tejeda, S. B. 1972 Studies of dynamic contact angles on solids. *J. Colloid Interface Sci.* **38**, 359–375.

Schwartz, L. W. 1989 Viscous flows down an inclined plane: Instability and finger formation. *Phys. Fluids* A **3**, 443–445.

Silvi, N. & Dussan V., E. B. 1985 On the rewetting of an inclined solid surface by a liquid. *Phys. Fluids* **28**, 5–7.

Smith, B. T. 1976 *Matrix Eigensystem Routines: Eispack Guide*. Springer.

Sreenivasan, S. & Lin, S. P. 1978 Surface tension driven instability of a liquid film down a heated incline. *Intl J. Heat Mass Transfer* **21**, 1517–1526.

Troian, S. M., Herbolzheimer, E., Safran, S. A. & Joanny, J. F. 1989 Fingering instabilities of driven spreading films. *Europhys. Lett.* **10**, 25–30.

Truong, J. C. & Wayner, P. C. Jr 1987 Effects of capillary and van der Waals dispersion forces on the equilibrium profile of a wetting liquid: theory and experiment. *J. Chem. Phys.* **87**, 4180–4188.

Wayner, P. C. Jr 1993 Spreading of a finite liquid film with a finite apparent contact angle by the evaporation/condensation process. *Langmuir* **9**, 294–299.

Williams, R. 1977 The advancing front of a spreading liquid. *Nature* **266**, 153–154.